A HIGH-RESOLUTION ROTATED GRID METHOD FOR CONSERVATION LAWS WITH EMBEDDED GEOMETRIES

CHRISTIANE HELZEL*, MARSHA J. BERGER†, AND RANDALL J. LEVEQUE‡

Abstract. We develop a second-order rotated grid method for the approximation of time dependent solutions of conservation laws in complex geometry using an underlying Cartesian grid. Stability for time steps adequate for the regular part of the grid is obtained by increasing the domain of dependence of the numerical method near the embedded boundary by constructing h-boxes at grid cell interfaces. We describe a construction of h-boxes that not only guarantees stability but also leads to an accurate and conservative approximation of boundary cells that may be orders of magnitude smaller than regular grid cells. Of independent interest is the rotated difference scheme itself, on which the embedded boundary method is based.

Key words. finite volume methods, conservation laws, Cartesian grids, irregular geometries

AMS subject classifications. 35L65, 65M06, 76M12

1. Introduction. We present a high-resolution Cartesian grid embedded boundary method for the approximation of hyperbolic conservation laws in complex geometries. A Cartesian grid approach is attractive, since away from the boundary it allows the use of standard high-resolution shock capturing methods that are more difficult to develop on unstructured (body fitted) grids. Embedded boundary grids allow a more automated grid generation procedure around complex objects, which is important especially for three-dimensional problems. The numerical challenge associated with a Cartesian grid embedded boundary approach is the so-called *small cell problem*. Near the embedded boundary the grid cells may be orders of magnitude smaller than regular Cartesian grid cells. Since standard explicit finite volume methods take the time step proportional to the size of a grid cell, this would typically require small time steps near an embedded boundary. We will describe a numerical method that overcomes the time step restriction, while seeking an accurate approximation near the embedded boundary as well as in the whole domain.

During the last decade, many different Cartesian grid embedded boundary methods have been developed. Several authors use a cell merging technique, where small irregular cut cells are merged together with a neighboring regular grid cell, see for instance Coirier and Powell [9] or Quirk [33]. An interesting variant of cell merging was suggested by Falcovitz et al. [14], who combined cell merging with dimension splitting. Chern and Colella [8] developed a flux redistribution procedure for front tracking methods. This approach was extended by Pember et al. [32] and Modiano and Colella [29] to overcome the small cell problem for an embedded boundary method. In [16], Forrer and Jeltsch suggested an embedded boundary method where all grid cells are handled as full cells. Grid cells near the boundary are updated in each time step to simulate a reflecting boundary. A similar approach was also suggested by Xu

Version of March 25, 2004

et al. [38]. Although the small cell problem is overcome by all of these approaches, the accuracy near the boundary is reduced. Some of the available methods (i.e. [16], [38]) are not conservative, although this error may be relatively small.

Alternatively one can use an implicit scheme at the cut cells, but unless this is the method of choice for the rest of the domain [31], this is an expensive alternative.

An accurate approximation near the boundary may in particular be important for the simulation of flow problems with moving objects. Cartesian grid methods for conservation laws in the presence of moving objects have for instance been studied in the literature by Falcovitz et al. [14] (using cell merging) and Forrer and Berger [15] (extending the approach presented in [16]). For the test case studied in those papers the two different methods produced a different solution structure. Since the motion of the embedded object depends on the numerical solution near the boundary, this may indicate a strong need for the development of more accurate embedded boundary methods.

Our approach to overcome the small cell problem is based on the so-called h-box method suggested by Berger and LeVeque [4], [5]. Here we will extend this method to a high-resolution scheme. The basic idea behind the h-box method is to approximate numerical fluxes at the interface of a small cell based on initial values specified over regions of length h, where h is the length of a regular grid cell. In order to obtain the required stability property, the flux differences at cut cells should be of the size of the small irregular cell. Here we develop a high-resolution rotated grid method that has this *cancellation property* of numerical fluxes. We first study our high-resolution rotated grid h-box method for regular Cartesian grids. Beside the development of an accurate embedded boundary method, the rotated grid method that is described in this paper may be of interest also for other applications. A crucial step in the development of this method is the definition of the left and right states that are used in the flux calculation of the rotated grid approach. We will show that for the approximation of the two-dimensional advection equation, our rotated grid h-box method is similar to an upwind method described by Roe and Sidilkover, see [34]. This implies an interesting optimality property. For the flux calculation a predictor-corrector approach, based on Colella's multidimensional high-resolution method described in [10], is used. We will show that in the context of a rotated grid method the predictor-corrector approach has advantages over other existing methods.

Several different rotated grid methods for the approximation of multi-dimensional systems of conservation laws can be found in the literature, see for instance [13], [18], [27], [34]. The main motivation for developing these methods was to reduce grid effects by calculating fluxes in a direction that depends on the solution structure instead of the grid. In [27], it was shown that rotated grid methods can lead to a sharper approximation of shock waves that are not aligned with the grid. In [26], LeVeque and Walder explored the use of first order accurate rotated grid h-box methods for the approximation of astrophysical applications. Nevertheless, what is really needed for the approximation of conservation laws are high-resolution methods that are second order accurate in smooth regions and lead to a sharp approximation of shock waves while spurious oscillations are suppressed. Compared to the rotated grid h-box method used in [26] as well as [4], [5], our new method uses a different h-box length, another definition of h-box values as well as a different flux calculation. All of those changes were necessary in order to obtain a method that is second order accurate for smooth solutions as well as stable for time steps with a Courant number of up to one.

In [2], we studied the construction of high-resolution h-box methods for the ap-

proximation of one-dimensional systems of conservation laws on irregular grids, see also [6] for earlier related work. This provides basic insight for the construction of an embedded boundary method in multi-dimensions. For the simpler one-dimensional situation we showed that our h-box method leads to a stable and second order accurate approximation of the advection equation on arbitrary irregular grids. Numerical results confirmed the same accuracy and stability properties for the approximation of the Euler equations. We are not familiar with other finite volume methods for one dimensional conservation laws on irregular grids that have the same accuracy and stability property. The large time step Godunov method of LeVeque described in [20], [21], [22] is related to the h-box method. This scheme allows larger time steps in the approximation of nonlinear systems of conservation laws by increasing the domain of influence of the numerical scheme. This is done in a wave propagation approach, in which waves are allowed to move through more than one mesh cell. The interaction of waves is approximated by linear superposition. At a reflecting boundary this method becomes more difficult than an h-box method especially in higher dimensions, since the reflection of waves at the boundary has to be considered for waves generated by Riemann problems away from the boundary, see [3]. In [30], Lemma 3.5, Morton showed that high-resolution versions of such a large time step method lead to a second order accurate approximation of the one-dimensional advection equation on a non-uniform grid only if the grid varies smoothly. Our second order h-box method does not require this smoothness assumption.

The rest of the paper is organized as follows. In section 2, we develop the high-resolution rotated grid h-box method for the approximation of conservation laws on regular two-dimensional Cartesian grids. It is a multidimensional method, in that it does not use dimension splitting. Our new embedded boundary rotated grid h-box method will be described in section 3. Throughout this paper we use the advection equation (with constant as well as varying velocity field) and the Euler equations of gas dynamics to illustrate the numerical method. Numerous simulations demonstrate the performance of our approach.

2. A high-resolution rotated grid method for regular Cartesian grids. We consider the approximation of a two dimensional system of conservation laws on a regular Cartesian grid. Under appropriate smoothness assumptions the equations can be written in the differential form

$$\frac{\partial}{\partial t}q(x,y,t) + \frac{\partial}{\partial x}f(q(x,y,t)) + \frac{\partial}{\partial y}g(q(x,y,t)) = 0, \tag{2.1}$$

where $q(x,y,t)$ is a vector of conserved quantities and $f(q(x,y,t))$ and $g(q(x,y,t))$ are vector valued flux functions. For the numerical approximation, we use a conservative finite volume method that takes the general form

$$Q_{i,j}^{n+1} = Q_{i,j}^n - \frac{\triangle t}{\triangle x}\left(F_{i+\frac{1}{2},j} - F_{i-\frac{1}{2},j}\right) - \frac{\triangle t}{\triangle y}\left(G_{i,j+\frac{1}{2}} - G_{i,j-\frac{1}{2}}\right). \tag{2.2}$$

The numerical fluxes F and G at the cell interfaces are calculated via a rotated grid approach with coordinate directions ξ and η and angle of rotation θ. In the new coordinate system the hyperbolic equation (2.1) takes the form

$$\frac{\partial}{\partial t}q(\xi,\eta,t) + \frac{\partial}{\partial \xi}\tilde{f}(q(\xi,\eta,t)) + \frac{\partial}{\partial \eta}\tilde{g}(q(\xi,\eta,t)) = 0, \tag{2.3}$$

with

$$\tilde{f}(q) = f(q)\cos(\theta) + g(q)\sin(\theta), \tag{2.4}$$

$$\tilde{g}(q) = -f(q)\sin(\theta) + g(q)\cos(\theta). \tag{2.5}$$

At each cell interface of the Cartesian grid we solve Equations (2.4) and (2.5) numerically. This gives the numerical fluxes $\tilde{F}$ and $\tilde{G}$. The numerical fluxes F and G that are used in the finite volume scheme (2.2) can then be obtained via the relations

$$F = \tilde{F}\cos(\theta) - \tilde{G}\sin(\theta) \tag{2.6}$$

$$G = \tilde{F}\sin(\theta) + \tilde{G}\cos(\theta). \tag{2.7}$$

The numerical fluxes $\tilde{F}$ and $\tilde{G}$ are calculated by solving Riemann problems for the one-dimensional equations

$$\frac{\partial}{\partial t}q + \frac{\partial}{\partial \xi}\tilde{f}(q) = 0 \tag{2.8}$$

$$\frac{\partial}{\partial t}q + \frac{\partial}{\partial \eta}\tilde{g}(q) = 0. \tag{2.9}$$

The crucial step in order to obtain an accurate high-resolution rotated grid method is the definition of left and right states of the conserved quantities that are used as initial values for the solution of Riemann problems in the ξ and η-direction respectively. We will derive a new rotated grid h-box method that is motivated by a multidimensional upwind method of Roe and Sidilkover, see [34]. For simplicity we first restrict our consideration to the approximation of the two-dimensional advection equation.

2.1. A rotated grid method for advective transport. Consider the two-dimensional advection equation with constant advection speed, i.e.

$$\frac{\partial}{\partial t}q(x,y,t) + u\frac{\partial}{\partial x}q(x,y,t) + v\frac{\partial}{\partial y}q(x,y,t) = 0. \tag{2.10}$$

In order to develop a high-resolution rotated grid method we want to use appropriate linear interpolation formulas to define the conservative quantities used in the flux calculations. Note that this was also the crucial step in developing high-resolution irregular grid h-box methods in the 1D case, see [2]. We will formulate the rotated grid method as an h-box method. The use of h-boxes allows simple geometric interpretations which will later be useful for the construction of the embedded boundary method. To make comparisons with other existing schemes easier, we first restrict our considerations to the case $0.5 \le u/v \le 2$. We will see below that our rotated grid h-box method generalizes in a straightforward way to arbitrary values of the advection speed. Our approach for finding the h-box values is motivated by multidimensional upwind methods described in Roe and Sidilkover [34], where the approximation of steady state solutions for the advection equation was considered. See also [36] and [37] for related work.

A geometric interpretation of a two-dimensional second order accurate upwind method for steady state problems is shown in Figure 2.1a. At each cell interface the conservative quantity that is used in the upwind scheme is defined by tracing back the characteristic at the midpoint of the cell interface (for instance A). Linear interpolation onto the Cartesian grid using C and D is used to find the values that are assigned
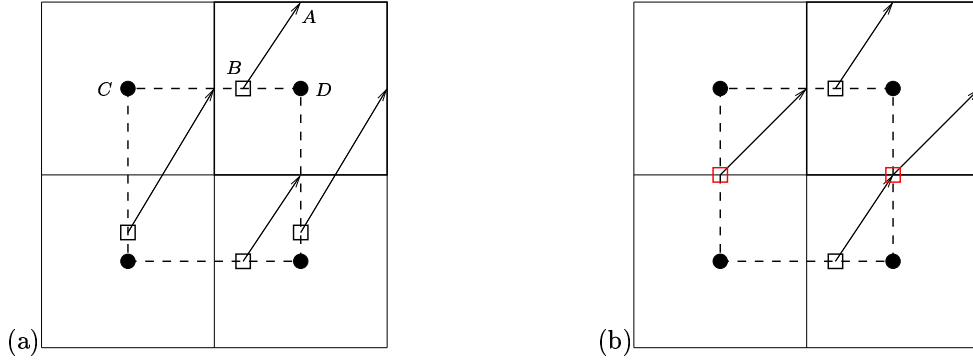
FIG. 2.1. *Schematic description of the advection algorithm suggested by Roe and Sidilkover [34]. (a) A second order residual results from interpolating to the values at the open squares. (b) The optimum first order method (N-scheme) results from moving each interpolation point to the midpoint of its interval, if initially it is more than half a length away from the center of the grid cell interface considered.*

to the characteristic. In [36, section 4.2.1] it was shown that the resulting upwind method is second order accurate for smooth steady-state solutions of the advection equation. However this scheme is not monotone and therefore not suitable for the approximation of discontinuous solutions. In [34], Roe and Sidilkover derived an optimal positive method, i.e. a first order accurate method with the smallest truncation error among all monotone schemes that use the same narrow stencil. A geometric interpretation of this method is illustrated in Figure 2.1b. The upwind points for the flux calculations $G_{i,j+\frac{1}{2}}$ and $G_{i,j-\frac{1}{2}}$ are obtained by characteristic interpolation while the upwind points used for the fluxes $F_{i-\frac{1}{2},j}$ and $F_{i+\frac{1}{2},j}$ are obtained by arithmetic averaging, i.e. the interpolation points for the calculation of the fluxes in the x-direction are moved upward. Assuming that the advection speeds satisfy $0.5 \leq u/v \leq 2$, fluxes are found by characteristic interpolation, if the interpolation point is at most a half grid cell length apart from the center of the cell interface (i.e. the G fluxes in Figure 2.1a), otherwise the interpolation point is moved and the corresponding fluxes are determined by averaging. This method is often called the N-scheme for its narrow stencil. Here we will discuss an interpretation of the N-scheme as a rotated grid h-box method that will lead to a natural extension to a high-resolution rotated grid method for time dependent problems.

Figure 2.2 shows an interpretation of the optimal positive scheme depicted in Figure 2.1b as an h-box method. At each cell interface we construct h-boxes in the characteristic direction, i.e. in direction (u, v) for the advection equation. In Figure 2.2a we show h-boxes that are used for the calculation of G fluxes. The interpolated point (illustrated in Figure 2.1b) that was used for the approximation of the G fluxes by the optimal positive scheme can also be obtained by calculating the corresponding h-box values based on the area fraction of the grid cells that are overlapped by the h-box. The N-scheme is obtained if we set the length of the h-boxes equal to

$$h = \sqrt{1 + (\min(|u|, |v|)/\max(|u|, |v|))^2}\triangle x. \qquad (2.11)$$

Note that in earlier work h-boxes of length $h = \triangle x = \triangle y$ were used, see [4], [5], [26]. For simplicity we assume $\triangle x = \triangle y$ throughout this paper. With the h-box length (2.11) the interpolation used for the calculation of the fluxes F by the optimal positive scheme (compare with Figure 2.1b) also has a geometric interpretation. Again
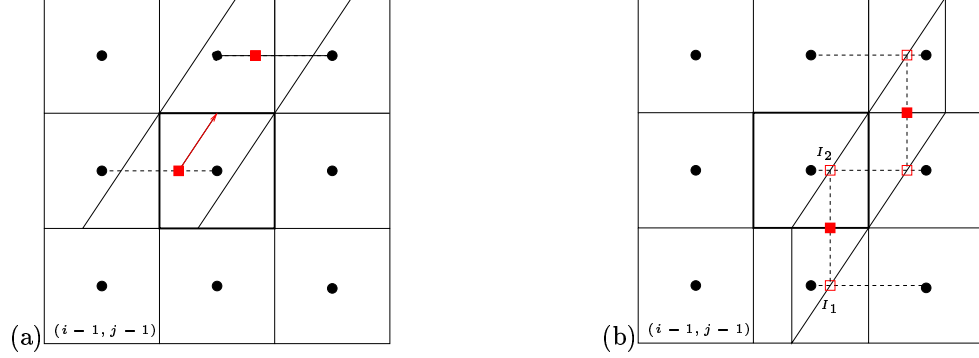
FIG. 2.2. *H-boxes in the ξ-direction for the calculation of the fluxes G and F respectively, that correspond to the optimal positive scheme.*

averaging over the h-boxes depicted in Figure 2.2b suggests using the average of the conserved quantities in the two grid cells that are overlapped by the h-box. This h-box method is stable for time steps that satisfy $CFL \leq 1$. To show stability we restrict our considerations to the case $u < v$, with $u, v \geq 0$. The method can be written in the form of a finite volume method

$$Q_{i,j}^{n+1} = Q_{i,j}^n - \frac{\triangle t}{\triangle x} u \left(Q_{i+\frac{1}{2},j}^L - Q_{i-\frac{1}{2},j}^L \right) - \frac{\triangle t}{\triangle y} v \left(Q_{i,j+\frac{1}{2}}^L - Q_{i,j-\frac{1}{2}}^L \right). \qquad (2.12)$$

The left h-boxes used in the above equation have the form:

$$Q_{i+\frac{1}{2},j}^L = \frac{1}{2} \left(Q_{i,j} + Q_{i,j-1} \right), \qquad Q_{i-\frac{1}{2},j}^L = \frac{1}{2} \left(Q_{i-1,j} + Q_{i-1,j-1} \right)$$
$$Q_{i,j+\frac{1}{2}}^L = \frac{u}{2v} Q_{i-1,j} + \left(1 - \frac{u}{2v} \right) Q_{i,j}, \quad Q_{i,j-\frac{1}{2}}^L = \frac{u}{2v} Q_{i-1,j-1} + \left(1 - \frac{u}{2v} \right) Q_{i,j-1}. \qquad (2.13)$$

Using these expressions we can rewrite the finite volume method (by again using $\triangle x = \triangle y$) into the form

$$Q_{i,j}^{n+1} = Q_{i,j}^n \left(1 - v \frac{\triangle t}{\triangle x} \right) + Q_{i,j-1}^n (v - u) \frac{\triangle t}{\triangle x} + Q_{i-1,j-1}^n u \frac{\triangle t}{\triangle x} \qquad (2.14)$$

All coefficients on the right hand side of Equation (2.14) are greater than or equal to zero assuming that $v \frac{\triangle t}{\triangle x} \leq 1$. In the general case, i.e. without the above assumptions on u and v, the time step restriction for stability takes the form $\triangle t \max(|u|, |v|)/\triangle x \leq 1$.

Other multi-dimensional methods for the advection equation can also be interpreted as rotated grid h-box methods. If we reduce the h-box length to

$$h = \triangle t \sqrt{u^2 + v^2},$$

then h-box values that are again calculated by averaging over piecewise constant cell averages of the conserved quantity take the form

$$Q_{i+\frac{1}{2},j}^L = Q_{i,j} - \frac{v \triangle t}{2 \triangle y}(Q_{i,j} - Q_{i,j-1}), \quad Q_{i-\frac{1}{2},j}^L = Q_{i-1,j} - \frac{v \triangle t}{2 \triangle y}(Q_{i-1,j} - Q_{i-1,j-1})$$
$$Q_{i,j+\frac{1}{2}}^L = Q_{i,j} - \frac{u \triangle t}{2 \triangle x}(Q_{i,j} - Q_{i-1,j}), \quad Q_{i,j-\frac{1}{2}}^L = Q_{i,j-1} - \frac{u \triangle t}{2 \triangle x}(Q_{i,j-1} - Q_{i-1,j-1}). \qquad (2.15)$$

The resulting rotated grid h-box method (2.12), (2.15) is equivalent with the corner transport upwind method (CTU) of Colella [10]. The CTU method can also be interpreted as wave propagation algorithm, see [23], [24]. This method is also first order accurate and stable for time steps that satisfy $CFL \leq 1$. In this paper we will concentrate on h-box methods with the fixed h-box length given by Equation (2.11).

Note that only in the special cases $u = v = 1$ (i.e. $\theta = \pi/4$), $u = 0$ or $v = 0$ does the optimal positive scheme of Roe and Sidilkover lead to a second order accurate approximation in space. For time dependent problems we want to obtain a high-resolution approximation by solving Riemann problems (defined by the h-box values) with a high-resolution method. Note that by using a Lax-Wendroff-type flux calculation (i.e. to get 2nd order in time) combined with the h-box method that corresponds to Roe and Sidilkover's approach we only get a second order accurate approximation in the special cases mentioned above.

There are high-resolution versions of the N-scheme, see for instance [37]. In order to combine the monotonicity property with second order accuracy a nonlinear scheme was constructed which blends between the N-scheme and the second order accurate non-monotone method. To retain monotonicity limiters are applied to the difference between the fluxes of the two methods. However, those methods cannot be interpreted as a rotated grid h-box method. As we will see in section 3, stability of the embedded boundary method relies on the use of a rotated grid method in which the upwind point can be interpreted as an approximation of the conserved quantities at the center of mass of an h-box. Therefore, we will now develop a new second order accurate rotated grid h-box method that has this property.

In order to obtain a second order accurate approximation with a rotated grid h-box method, the h-box values have to be calculated by appropriate linear interpolation. Our aim is to construct a high-resolution rotated grid h-box method that leads to second order accurate results for smooth solutions and avoids spurious oscillations for the approximation of discontinuities. We will derive such a scheme by using slope limiters in our interpolation scheme. If all slopes are set to zero, our scheme will reduce to the optimal positive scheme of Roe and Sidilkover. Figure 2.2b shows a description of the interpolation that is used to obtain the h-box values. We calculate the conserved quantities assigned to the left h-box by first determining the conserved quantities at the points I_1 and I_2 shown in the figure. Those values are in the unlimited case obtained by linear interpolation between neighboring grid cell values (e.g. $Q_{i,j}$ and $Q_{i+1,j}$ are used to calculate the conserved quantities at I_2). The conservative quantities assigned to the h-box are then obtained as the arithmetic average between the conserved quantities at the points I_1 and I_2. Note that the h-box values can be considered as a linear interpolation at the center of mass of the h-box (i.e. the little filled squares marked in Figure 2.2 are located at the center of mass of the h-box). In the case shown in Figure 2.2a, simple averaging over the region overlapped by the h-box is equivalent to linear interpolation to the center of mass of the h-box. The resulting h-box values can be used to construct second order accurate methods with appropriate second order flux formulas. In this case no slope limiting in the interpolation step for the calculation of the h-box values is necessary.

To avoid unphysical oscillations near discontinuities (even for the first order update) we include slope limiters into the interpolation process used for h-box values of the form indicated in Figure 2.2b. This is described in the next section. Once the h-box values are defined we can calculate the fluxes in the ξ and η-directions by a first order or a high-resolution method. This is analogous to the one-dimensional

irregular grid h-box method described in [2]. To obtain flux limiters that are needed by a high-resolution flux calculation, we construct an additional h-box on each side.

2.2. Slope limiters for the interpolation process. In this section we will restrict our considerations to the approximation of the advection equation with positive advection speed u, v and assume $v > u$. We choose our ξ-direction of the rotated grid method to be aligned with the constant velocity field. For the advection equation this implies that we do not have to calculate flux components in the η-direction. Our interpolation method for the calculation of the h-box values requires the use of slope limiters to avoid unphysical oscillations near discontinuities. Such a slope limiter is already necessary even if the fluxes are calculated with the first order upwind method, and we therefore restrict our considerations in this subsection to this case.

Our numerical method can be written in the conservative form (2.2), with

$$F_{k+\frac{1}{2},j} = uQ^L_{k+\frac{1}{2},j}, \quad k \in \{i-1, i\}$$
$$G_{i,k+\frac{1}{2}} = vQ^L_{i,k+\frac{1}{2}}, \quad k \in \{j-1, j\}$$

The left h-box values are

$$Q^L_{k+\frac{1}{2},j} = \frac{1}{2}(Q_{k,j-1} + Q_{k,j}) + \frac{1}{2}\left(\tilde{s}_{k+\frac{1}{2},j-1} + \tilde{s}_{k+\frac{1}{2},j}\right)d_1, \ d_1 = \frac{1}{2} - \frac{u}{2v}, \ k \in \{i-1, i\}$$
$$Q^L_{i,k+\frac{1}{2}} = (1 - d_2)Q_{i,k} + d_2 Q_{i-1,k}, \ d_2 = \frac{u}{2v}, \ k \in \{j-1, j\}.$$

$$(2.16)$$

In the above formulas d_1 is the distance of the interpolated point I_1 or I_2 to the center of mass of the grid cell in which this point lies, compare with Figure 2.2b. The value d_2 corresponds to the distance of the center of mass of an h-box to the center of mass of a grid cell in situations depicted in Figure 2.2a. The $\tilde{s}$ terms describe limited slopes used in the interpolation process as described below. The unlimited slope corresponds to a slope obtained by linear interpolation between neighboring grid cells in the x-direction, i.e.

$$s_{i+\frac{1}{2},j} = (Q_{i+1,j} - Q_{i,j})/\triangle x.$$

Our aim is to find appropriate slope limiters, such that the resulting rotated grid method (with upwind fluxes) avoids oscillations near discontinuities.

For the approximation of the advection equation with constant advection speed $v > u > 0$ on a grid with $\triangle x = \triangle y$, our rotated grid finite volume method takes the form

$$
\begin{aligned}
Q^{n+1}_{i,j} =& Q^n_{i,j} - \frac{\triangle t}{\triangle x}u(Q^L_{i+\frac{1}{2},j} - Q^L_{i-\frac{1}{2},j}) - \frac{\triangle t}{\triangle x}v(Q_{i,j+\frac{1}{2}} - Q_{i,j-\frac{1}{2}}) \\
=& Q^n_{i,j} - \frac{\triangle t}{\triangle x}u\Big[\frac{1}{2}(Q_{i,j-1} + Q_{i,j}) - \frac{1}{2}(Q_{i-1,j-1} + Q_{i-1,j}) \\
& + \frac{1}{2}\left(\tilde{s}_{i+\frac{1}{2},j-1} + \tilde{s}_{i+\frac{1}{2},j}\right)d_1 - \frac{1}{2}\left(\tilde{s}_{i-\frac{1}{2},j-1} + \tilde{s}_{i-\frac{1}{2},j}\right)d_1\Big] \\
& - \frac{\triangle t}{\triangle x}v\Big[(1 - d_2)(Q^n_{i,j} - Q^n_{i,j-1}) + d_2(Q^n_{i-1,j} - Q^n_{i-1,j-1})\Big]
\end{aligned}
$$

$$(2.17)$$

Setting all the $\tilde{s}$ terms in (2.17) equal to zero would lead to the monotone method suggested by Roe and Sidilkover. However, our main goal is the construction of a

second order rotated grid method and we therefore want to allow slopes that are not equal to zero wherever this is possible. In regions where the solution is smooth neighboring slopes would typically have about the same size, i.e. we have in particular

$$s_{i+\frac{1}{2},j-1} \approx s_{i-\frac{1}{2},j-1} \quad \text{and} \quad s_{i+\frac{1}{2},j} \approx s_{i-\frac{1}{2},j}. \tag{2.18}$$

The presence of such slopes in (2.17) would not destroy the monotonicity. Near discontinuities we need to use a slope limiter to enforce a relation of the form (2.18) to hold for the limited slopes. The relation (2.18) motivates the use of a two-sided slope limiter. This can be seen in the following way: In grid cell (i, j) the relation $\tilde{s}_{i+\frac{1}{2},j} \approx \tilde{s}_{i-\frac{1}{2},j}$ suggests using a left-sided slope limiter in order to limit the slope $s_{i+\frac{1}{2},j}$. This can for instance be done by using a minmod limiter (see for instance [25]) that can be written in the form

$$\text{minmod}(s_{i+\frac{1}{2},j}, s_{i-\frac{1}{2},j}). \tag{2.19}$$

In grid cell $(i + 1, j)$ the limited slope should satisfy $\tilde{s}_{i+\frac{1}{2},j} \approx \tilde{s}_{i+\frac{3}{2},j}$, which suggests using a right-sided slope limiter, for instance

$$\text{minmod}(s_{i+\frac{1}{2},j}, s_{i+\frac{3}{2},j}). \tag{2.20}$$

The limited slope $\tilde{s}_{i+\frac{1}{2},j}$ is used to calculate the upwind point needed to obtain the numerical flux $F_{i+\frac{1}{2},j}$. In a conservative finite volume method we use the same flux $F_{i+\frac{1}{2},j}$ to update the cell average of the conserved quantity in grid cell (i, j) and $(i + 1, j)$. Therefore we need a combination of the left- and right-sided slope limiter. This can be obtained by applying the minmod function to the two values (2.19) and (2.20) which results in the two-sided limiter

$$\tilde{s}_{i+\frac{1}{2},j} = \text{minmod}(s_{i-\frac{1}{2},j}, s_{i+\frac{1}{2},j}, s_{i+\frac{3}{2},j}). \tag{2.21}$$

Our numerical experiments show that it is indeed necessary to consider the slopes from both sides of the grid cell to obtain effective slope limiters. The next test calculation will illustrate this.

EXAMPLE 2.1. *We consider the advection equation with advection speeds $u = 0.8$, $v = 1$. The initial values contain a disk with radius 0.2 located at $(x, y) = (0.25, 0.25)$ and a square with center initially located at $(0.65, 0.65)$.*

Figure 2.3b shows numerical results at time $t = 0.2$ of the rotated grid method with first order upwind flux without the use of slope limiters in the interpolation step where the h-box values are defined. This clearly shows oscillations near discontinuities. For the calculation shown in (c) we used a one-sided slope limiter of the form (2.20). This limiter is clearly a good choice for the test problem considered, although small oscillations are still visible. For the calculation shown in (d) we used a one-sided limiter of the form (2.19), which turns out to be quite ineffective. In (a) we show the results obtained by using the two-sided limiter (2.21). The same limiting process can be applied in more general situations, e.g. advective transport with variable velocity field or the approximation of systems of conservation laws.

2.3. Verification of the high-resolution rotated grid method for advective transport problems. In order to approximate the 2D advection equation with a rotated grid method, we choose the ξ-direction to be aligned with the velocity field.
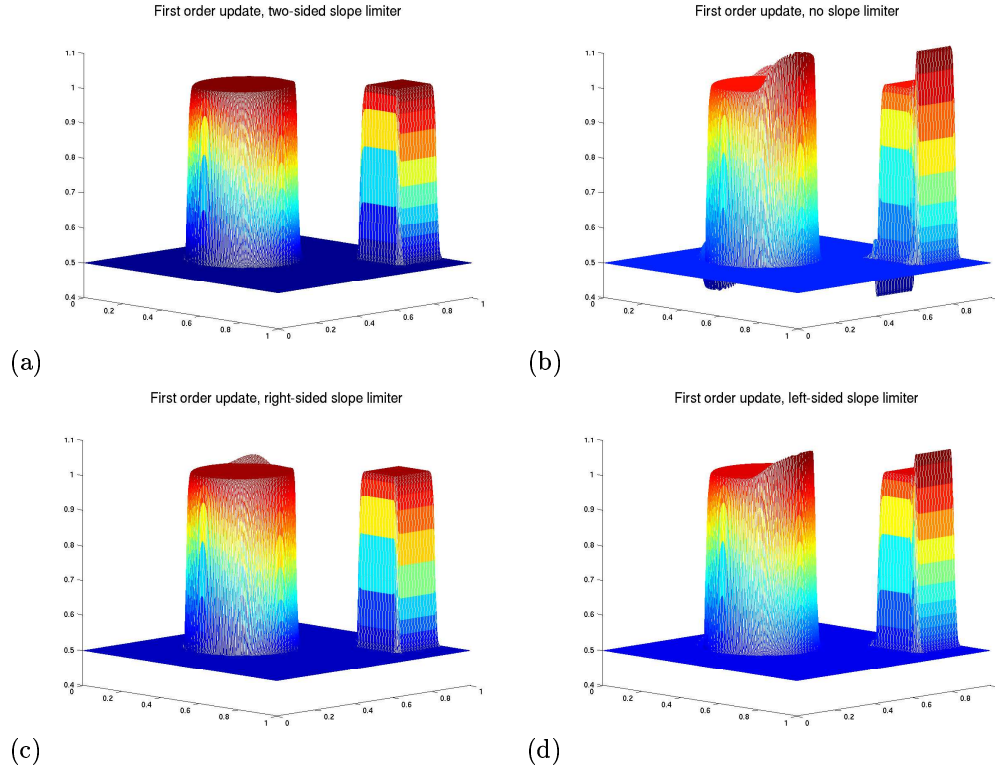
First order update, two-sided slope limiter

First order update, no slope limiter

(a)

(b)

First order update, right-sided slope limiter

First order update, left-sided slope limiter

(c)

(d)

FIG. 2.3. *Test calculation of Example 2.1 with different slope limiters. All calculations use a first order flux calculation but linear interpolation to determine the h-box values. 400×400 grid cells, $CFL_h \approx 0.95$, $t = 0.2$.*

The fluxes in the η-direction are then equal to zero and we do not have to construct h-boxes in this orthogonal direction. At each cell interface we approximate

$$q_t + \sqrt{u^2 + v^2}q_\xi = 0,$$

where u and v denote the advection speed. Let $\tilde{F}$ be approximated by the Lax-Wendroff flux formula

$$\tilde{F} = \frac{1}{2}\sqrt{u^2 + v^2}(Q^L + Q^R) - \frac{1}{2}\frac{\triangle t}{h}(u^2 + v^2)(Q^R - Q^L),$$

where Q^L and Q^R are the h-box values at the grid cell interface considered and h is the length of the h-box. We obtain the following accuracy result.

PROPOSITION 1. *Consider the approximation of sufficiently smooth solutions of the two-dimensional advection equation by a rotated grid h-box method. The direction of the h-boxes are aligned with the velocity field. If the h-box values are calculated by (unlimited) linear interpolation as described in (2.16) and the fluxes $\tilde{F}$ are approximated by the Lax-Wendroff method, then the resulting finite volume method is second order accurate.*

We omit the proof which is based on Taylor series expansion and instead show numerical results for a slightly more general situation, where the advection speed is locally varying.

EXAMPLE 2.2. **Solid body rotation.** *The time independent velocity field for solid body rotation on* $[0, 1] \times [0, 1]$ *is given by*

$$u = -(y - 0.5), \quad v = (x - 0.5).$$

As initial values we consider a smooth hump of the form

$$q(x, y, 0) = \frac{1}{4} \left(1 + \cos\left(\pi r(x, y)\right)\right),$$

with

$$r(x, y) = \min\left(\sqrt{(x - x_0)^2 + (y - y_0)^2}, r_0\right) / r_0.$$

The parameters are set to $x_0 = 0.25$, $y_0 = 0.5$, $r_0 = 0.15$. *At time* $t = 2\pi$, *i.e. after one rotation, the exact solution agrees with the initial values.*
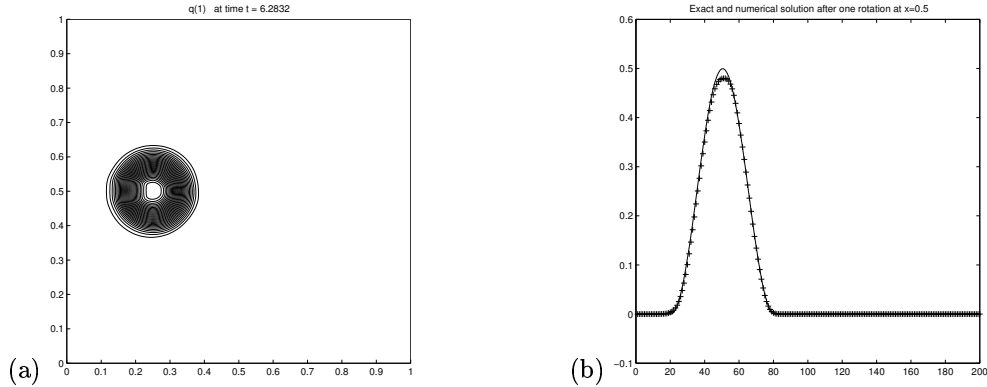

(a)   (b)

FIG. 2.4. *Solution of the rotating flow problem after one rotation using high-resolution flux formulas on a grid with* 200×200 *mesh cells. (a) Contour plot of solution, (b) comparison of exact and numerical solution after one full rotation at* $y = 0.5$.

Figure 2.4 shows numerical results for the rotating flow problem. In Figure 2.4a, a contour plot of the numerical solution is shown after one full rotation. In 2.4b we show a one-dimensional slice of the numerical solution at $y = 0.5$ together with the exact solution (solid line). Table 2.1 shows the L_1-errors as well as the experimental order of convergence (EOC) after one rotation. For this smooth solution, results were obtained

(mx, my) / EOC	new rotated grid method with Lax-Wendroff flux	Roe and Sidilkover method with Lax-Wendroff flux
(100,100)	0.27624	0.33239
(200,200)	7.88745-2	0.12841
EOC	1.81	1.37
(400,400)	2.18381-2	5.60114d-2
EOC	1.85	1.20
(800,800)	5.83500d-3	2.63392d-2
EOC	1.90	1.09

TABLE 2.1
Accuracy study for the rotating flow problem.

using our new rotated grid method that is based on h-box values obtained by linear interpolation as described above and a Lax-Wendroff flux calculation. The numerical test confirms second order convergence. We also show the error and numerical order of convergence for a test calculation where we used h-box values that correspond to the optimal positive scheme of Roe and Sidilkover combined with a Lax-Wendroff flux calculation. As expected this leads to a first order accurate approximation.

2.4. A rotated grid method for systems of conservation laws. We now extend our rotated grid method to the approximation of two-dimensional systems of conservation laws. To illustrate the performance of the method we consider the Euler equations of gas dynamics. In the case of two spatial dimensions, the Euler equations take the form

$$\rho_t + (\rho u)_x + (\rho v)_y = 0$$
$$(\rho u)_t + (\rho u^2 + p)_x + (\rho uv)_y = 0$$
$$(\rho v)_t + (\rho uv)_x + (\rho v^2 + p)_y = 0$$
$$E_t + (u(E + p))_x + (v(E + p))_y = 0,$$

where (u, v) represents the velocity, ρ the density, p the pressure and E the energy. We use the ideal gas equation of state

$$E = \frac{p}{\gamma - 1} + \frac{1}{2}\rho(u^2 + v^2).$$

The approximation of two-dimensional systems of conservation laws with a rotated grid method requires the construction of h-boxes in the ξ and η-direction. The conserved quantities that are assigned to the h-boxes can be calculated by an interpolation procedure analogous to that of the advection equation, with the interpolation now performed for a vector of conserved quantities. Slope limiters for each conserved variable are used to prevent unphysical oscillations near discontinuities. Once the h-box values are known, we perform the flux calculation by using a *predictor-corrector method*. In the special case where the rotated grid is aligned with the Cartesian grid coordinates, the predictor corrector method agrees with Colella's multidimensional upwind method described in [10]. Using a predictor-corrector method the numerical flux $\tilde{F}$ (i.e. the numerical flux for Equation (2.4), at the grid cell interface $(x_{i+\frac{1}{2}}, y_j)$) is calculated as

$$\tilde{F}_{i+\frac{1}{2}, j} = \tilde{F}\left(Q^L_{i+\frac{1}{2}, j}(x_{i+\frac{1}{2}}, y_j, t^{n+\frac{1}{2}}), Q^R_{i+\frac{1}{2}, j}(x_{i+\frac{1}{2}}, y_j, t^{n+\frac{1}{2}})\right). \qquad (2.22)$$

In the predictor step we estimate the conserved quantity at the grid cell interface at time $t^{n+\frac{1}{2}}$. Those values are then used in the corrector step (2.22). Analogous predictor-corrector steps are also necessary for the approximation of the $\tilde{G}$ fluxes at the cell interface $(x_{i+\frac{1}{2}}, y_j)$ as well as for the approximation of $\tilde{F}$ and $\tilde{G}$ fluxes at cell interfaces $(x_i, y_{j+\frac{1}{2}})$. Using Taylor series expansion, we find that

$$\begin{aligned}
Q^{L,R}_{i+\frac{1}{2}, j}(x_{i+\frac{1}{2}}, y_j, t^{n+\frac{1}{2}}) &= Q^{L,R}_{i+\frac{1}{2}, j} \pm \frac{\triangle\xi}{2}q_\xi + \frac{\triangle t}{2}q_t \\
&= Q^{L,R}_{i+\frac{1}{2}, j} \pm \frac{\triangle\xi}{2}q_\xi - \frac{\triangle t}{2}\left(\frac{\partial}{\partial\xi}\tilde{f} + \frac{\partial}{\partial\eta}\tilde{g}\right) \\
&= Q^{L,R}_{i+\frac{1}{2}, j} + \left(\pm\frac{\triangle\xi}{2} - \frac{\triangle t}{2}\tilde{A}\right)q_\xi - \frac{\triangle t}{2}\frac{\partial}{\partial\eta}\tilde{g}(q) + \mathcal{O}(\triangle\xi^2, \triangle t^2).
\end{aligned}$$

Here $\tilde{A}$ is the Jacobian matrix of the flux $\tilde{f}$ from Equation (2.8) with $\tilde{f}$ calculated by (2.4). The distance $\triangle\xi$ is equivalent to the length of the h-box constructed in ξ-direction. The predictor step can be performed in the two successive steps

$$\hat{Q}^{L,R}_{i+\frac{1}{2},j} = Q^{L,R}_{i+\frac{1}{2},j} + \left(\pm\frac{\triangle\xi}{2} - \frac{\triangle t}{2}\tilde{A}\right)q_\xi \qquad (2.23)$$

$$Q^{n+\frac{1}{2}}_{i+\frac{1}{2},j} = \hat{Q}^{L,R}_{i+\frac{1}{2},j} - \frac{\triangle t}{2}\frac{\partial}{\partial\eta}\tilde{g}(q). \qquad (2.24)$$

In the first step we reconstruct the state from the cell center to the cell interface by taking into account only the characteristics that point toward the interface. This is done by analogy to Colella's grid aligned method described in [10]. In the second step we include a transverse flux difference. This step is necessary in order to obtain stability for time steps up to a Courant number of one. (Note that in a rotated grid method for the advection equation, where the coordinate direction is aligned with the characteristic direction, the transverse flux component would be equal to zero, so we did not have to include a transverse flux difference.) In order to incorporate the transverse flux difference into the predictor step, we need to solve Riemann problems in the η-direction. We first have to define appropriate initial values say Q_1, Q_2 and Q_3. For the intermediate value we use our h-box value, i.e. $Q_2 = Q^{L,R}_{i+\frac{1}{2},j}$. The definition of the other two values is indicated in Figure 2.5. From the center of mass of each
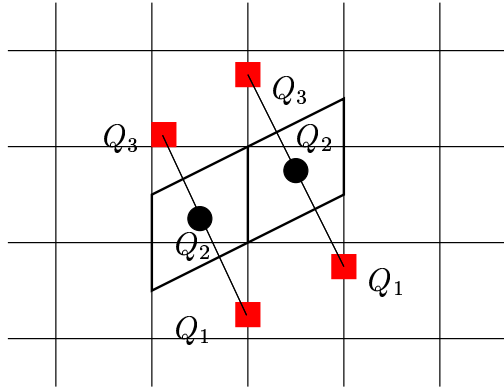

FIG. 2.5. *Schematic description of points defined for the calculation of the transverse flux difference.*

h-box we find points along a line in the transverse direction that have the distance h from the center of mass. The conserved quantities that are assigned to those points are obtained by interpolation between the four closest neighboring grid cells of the underlying Cartesian grid. Then the transverse flux difference can be approximated by $(\tilde{G}(Q_2, Q_3) - \tilde{G}(Q_1, Q_2))/h$, where $\tilde{G}$ is the numerical flux obtained by solving Riemann problems for Equation (2.9).

Below we perform several test calculations, using model problems that have been studied in the literature with grid aligned finite volume methods. The numerical results obtained with our rotated grid h-box method compare well with those obtained by other state of the art methods for hyperbolic problems.

Note that in general situations, we do not know the best choice for the direction of the rotated grid a priori. For the 2D Euler equations, different approaches may

be possible. A simple approach is to choose the ξ-direction aligned with the local velocity field. However, if we want to approximate shock waves that are not aligned with the grid a better choice for the rotated grid might be to choose the ξ-direction aligned with the pressure gradient. With such an approach we hope to get sharper approximation of shock waves. By comparing first order accurate methods a much sharper approximation of shock waves that are not aligned with the grid can indeed be obtained by using a rotated grid method that is aligned with the shock instead of a grid aligned method, see [27]. However, high-resolution grid aligned methods lead to very accurate approximation of shock waves that are not aligned with the grid and we do not see any further improvement by using our rotated grid method. Instead we will see that our rotated grid method compares well with grid aligned high-resolution methods.

We first demonstrate the performance of our high-resolution rotated grid method for a two-dimensional Riemann problem, as suggested in [35]. Note that this test case was also considered in [28], where several numerical methods were compared.

EXAMPLE 2.3. *We approximate the solution of the two-dimensional Euler equations with piecewise constant initial values. Let the index indicate the quadrant, then the initial values have the following form.* $p_1 = 0.4, \rho_1 = 0.5313, u_1 = 0.0, v_1 = 0.0, p_2 = 1.0, \rho_2 = 1.0, u_2 = 0.7276, v_2 = 0.0, p_3 = 1.0, \rho_3 = 0.8, u_3 = 0.0, v_3 = 0.0, p_4 = 1.0, \rho_4 = 1.0, u_4 = 0.0, v_4 = 0.7276.$ *The ratio of specific heat is set to* $\gamma = 1.4$ *and the computational domain is* $[0,1] \times [0,1]$. *All neighboring Riemann problems resulting from this initial value problem lead to shock wave solutions.*

Figure 2.6 shows results of a numerical approximation of density and pressure. To
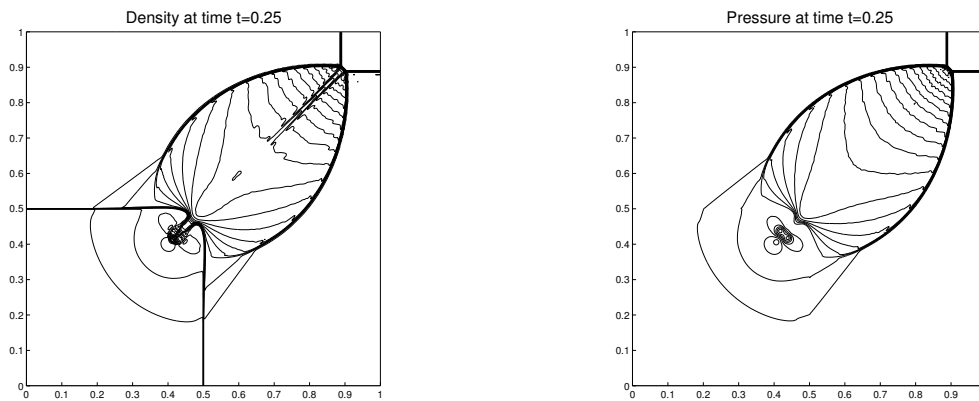

FIG. 2.6. *Contour plots of density and pressure for Example 2.3.* 400×400 *grid cells. The direction of the rotated grid is determined from the pressure gradient.*

make comparison with the schemes shown in [28] possible, we use the same resolution, i.e. a grid with 400×400 mesh cells. With our rotated grid method, near shock waves the grid direction is aligned with the pressure gradient while the direction of the underlying Cartesian grid is used away from discontinuities. We get a sharp approximation of the shock structure and also demonstrate that our limiting avoids unphysical oscillations.

Next we perform an accuracy study by comparing the results of a 2D radially symmetric problem with the numerical solution of a one dimensional calculation with geometric source term that models the radial symmetry.

EXAMPLE 2.4. *We consider the 2D Euler equations with initial values that have zero velocity. Initial values for density and energy are given by the smooth function*

$$\rho(x, y, 0) = E(x, y, 0) = \begin{cases} 1 - 0.1(\cos(4\pi r) - 1) & : \quad 0 < r < 0.5 \\ 1 & : \quad r \geq 0.5, \end{cases}$$

with $r = \sqrt{x^2 + y^2}$. The computational domain is $[0, 1] \times [0, 1]$, with solid wall boundary condition at $x = 0$ and $y = 0$.

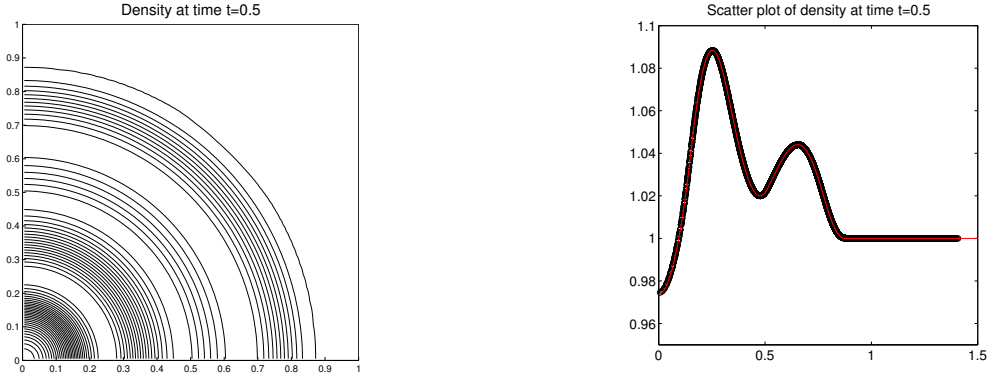Numerical results for this test problem are shown in Figure 2.7. An experimental

FIG. 2.7. *Solutions of Example 2.4 on a grid with 100×100 mesh cells. (a) Contour plot of density, (b) Scatter plot of 2D solution together with 1D reference solution (solid line). Second order method without limiters. The ξ-direction of the rotated grid is aligned with the radial direction.*

convergence study is shown in Table 2.2, which confirms that our method is second order accurate also for this nonlinear system. Now the radial direction describes the ξ-direction for our rotated method.

(mx, my) / EOC	ρ	ρu	E
(50,50)	1.9630d-4	1.3794d-4	2.7403d-4
(100,100)	5.0255d-5	3.5021d-5	7.0454d-5
EOC	1.96	1.98	1.96
(200,200)	1.3376d-5	9.2185d-6	1.8726d-5
EOC	1.91	1.93	1.91

TABLE 2.2

Accuracy study for Example 2.4 using the second order rotated grid method without limiters. A rotated grid method was used in which the ξ-direction is aligned with the radial direction. Errors are calculated in the L_1 norm. The 1D reference solution was calculated on a grid with 40000 mesh cells. For the 2D simulation we used a discretization with $\triangle t = \triangle x = \triangle y$, which leads to $CFL \approx 0.8$.

This test case was also considered in [24], where results for the high-resolution wave propagation algorithm were shown. Our results are approximately equivalent to the results documented in [24]. The wave propagation method or Colella's grid aligned method [10] as well as other grid aligned methods are of course less expensive than our rotated grid method. We need to solve about twice as many Riemann problems as these other methods. However, our main motivation for the development of the high-resolution rotated grid method is to overcome the small cell problem for Cartesian grid methods with embedded boundaries. In that case, we only want to use

the rotated grid method near the embedded boundary, while a classical grid aligned method can be used away from the boundary.

3. The embedded boundary method. Based on our high-resolution rotated grid method we now describe a high-resolution rotated grid embedded boundary method. The resulting method is a refinement of the embedded boundary method of Berger and LeVeque [4], [5]. We assume that the embedded boundary is described by a piecewise linear segment that cuts through each boundary cell once. Then each irregular grid cell is a polygon with at most five sides. Thus a finite volume method has the form

$$Q_{i,j}^{n+1} = Q_{i,j}^n - \frac{\Delta t}{a_{i,j}} \left(\ell_{i+\frac{1}{2}} F_{i+\frac{1}{2},j} - \ell_{i-\frac{1}{2}} F_{i-\frac{1}{2},j} + \ell_{j+\frac{1}{2}} G_{i,j+\frac{1}{2}} - \ell_{j-\frac{1}{2}} G_{i,j-\frac{1}{2}} + \ell_{i,j} H_{i,j} \right).$$

Here F and G denote the fluxes in the x and y-direction respectively. H is the flux per unit time through the irregular side of the cell, the solid wall boundary. The value $a_{i,j}$ describes the size of the grid cell and $\ell_{i+\frac{1}{2}}$ is the length of the interface between cell (i, j) and $(i+1, j)$. Note that ℓ may be zero if the corresponding grid cell interface is completely covered by the boundary. In order to obtain a conservative boundary flux, we construct h-boxes normal to the boundary. This is illustrated in Figure 3.1a. To allow time steps based on a CFL condition that is appropriate for the regular part of the grid, the domain of dependence has to be large enough. By analogy with our rotated grid method for regular Cartesian grids, we use h-boxes of length described in Equation (2.11).

At the embedded boundary the h-box method retains stability by constructing a finite volume scheme where the flux differences in each cut cell are of the order of the size of the small cell. This balances the term $a_{i,j}$ in the denominator. The direction normal to the boundary segment is the η-direction of our rotated grid method. For a small triangular shaped cell the h-boxes constructed in the η-direction are shown in Figure 3.1a, b, c. Those h-boxes overlap except on an area of the size of the small grid cell. In Figure 3.1d and e, we show the h-boxes constructed in orthogonal direction (the ξ-direction of our rotated grid method). Those h-boxes also overlap except on an area of the size of the small cell. Since the flux calculation is Lipschitz continuous, this gives us the cancellation property needed to obtain stability in the small cell. A construction of the boundary h-boxes in direction normal to the boundary allows us to construct a conservative method.

In the two-dimensional case we do not have a stability proof of our method at cut cells. However, the heuristic argument given above is a generalization of the stability argument developed in the one-dimensional case. We have proved stability of the second order accurate h-box method on one-dimensional irregular grids in [2].

In order to obtain high-accuracy near the boundary of an embedded object, we have to find accurate interpolation formulas for the calculation of the h-box values. Furthermore, these h-box values have to be constructed in a way that avoids oscillations near discontinuities. This can be obtained by a generalization of the limiting described in section 2.2.

In order to measure the accuracy of our embedded boundary method at the boundary as well as inside the domain, we use two different norms. Inside the domain we can calculate the error with a standard L_1-norm of the form

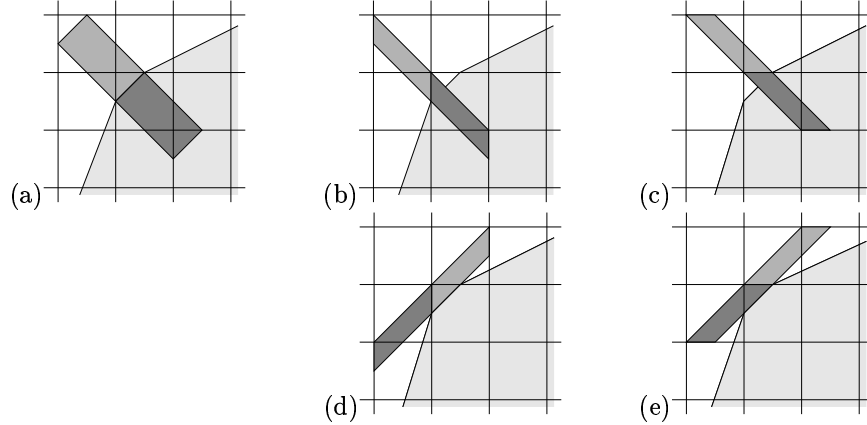$$E_d = \frac{\sum_{i,j} |Q_{i,j} - q(x_i, y_j)| a_{i,j}}{\sum_{i,j} |q(x_i, y_j)| a_{i,j}}.$$

FIG. 3.1. (a) Construction of a boundary h-box, i.e. in η-direction of our rotated grid. (b), (c) Construction of h-boxes in η-direction. (d), (e) Construction of h-boxes in ξ-direction.

Here $Q_{i,j}$ is the numerical solution in grid cell (i,j) and $q(x_i, y_j)$ is the exact solution at the center of mass of this grid cell. The area of the grid cell (i,j) is $a_{i,j}$. To measure the boundary error we sum over all cut cells and calculate the norm

$$E_b = \frac{\sum_{(i,j) \in K} |Q_{i,j} - q(x_i, y_j)| b_{i,j}}{\sum_{(i,j) \in K} |q(x_i, y_j)| b_{i,j}},$$

where $b_{i,j}$ is the length of the boundary segment in grid cell (i,j). K is the set of all cut cells along the embedded boundary.

A second order accurate approximation of the solution over the whole domain can be obtained, even if the boundary is only approximated with first order accuracy. This is due to the lower dimensionality of the boundary segment, see Gustafsson [17]. However, in several applications one may be especially interested in the solution near the boundary. In such cases an accurate boundary treatment is essential. We start the description of our embedded boundary method by presenting an approach for the advection equation with variable velocity field. The velocity field is described by a stream function that may be given by an analytical formula or by a numerical approximation. By studying advective transport problems first, we again only have to construct h-boxes for our rotated grid method in the direction aligned with the velocity field.

3.1. Advection equation. In this subsection we construct an embedded boundary rotated grid method for the approximation of advective transport problems with variable velocity field. We assume that the velocity field near the boundary is tangential to the boundary and may be given by a stream function. Such a situation may for instance describe the advection of a tracer through a field with irregular inclusions to model porous media flow. This situation can be simulated by a rotated grid h-box method with h-boxes in the ξ-direction only.

By analogy with our rotated grid h-box method for regular Cartesian grids, we want to construct h-box values that represent a linear interpolation of the conserved quantities to the center of mass of the h-boxes. We first calculate for each h-box the area fractions of all polygons that represent the intersection of the h-box with the underlying Cartesian grid cells that are overlapped by the h-box. As is clear from

Figure 3.1d and e, an h-box in the ξ-direction intersects at most two Cartesian grid cells. We calculate the center of mass of these two polygons. We also need to know the center of mass of the underlying grid cells that are overlapped by the h-box as well as a gradient of the conserved quantities in each grid cell. Using this information we can interpolate the conserved quantities at the center of mass of the polygons that represent the intersection of the h-box with the grid cells. The conserved quantity that represents an interpolation at the midpoint of the h-box can then be obtained as an area-weighted sum of the interpolated values at the center of mass of the polygon. In order to calculate the gradients of the conserved quantities in grid cells near the boundary, we use a least square procedure. A limiter is used to prevent oscillations near discontinuities.

To test our embedded boundary method we first consider advective transport inside an annulus.

EXAMPLE 3.1. *We consider solid body rotation inside an annulus defined by two concentric circles. The radius of the inner circle is $R_1 = 0.75$ and the radius of the outer circle is $R_2 = 1.25$. The annulus is embedded into a Cartesian grid of the size $[-1.5, 1.5] \times [-1.5, 1.5]$. We use initial values of the form*

$$q(x, y, t) = w(\theta - \pi/2)$$

with

$$w(\theta) = 0.5 \left\{ erf\left(\frac{\pi/6 - \theta}{\sqrt{4/100}} \right) + erf\left(\frac{\pi/6 + \theta}{\sqrt{4/100}} \right) \right\}.$$

The velocity field describing solid body rotation was obtained using the stream function

$$\psi(x, y) = 0.2\pi (R_2^2 - r^2),$$

with $r = (x^2 + y^2)^{1/2}$. One rotation is completed at time $t = 5$.

Figure 3.2 shows contour plots of the numerical solution at different time steps. The solution at the two boundaries is shown in Figure 3.3. We used our second order
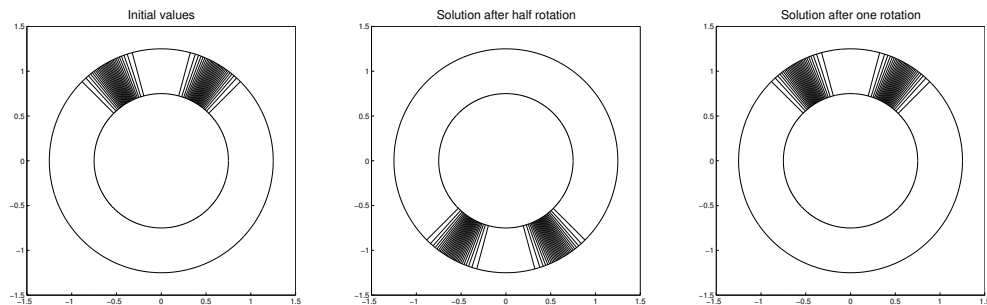

FIG. 3.2. *Solution of the annulus test problem on a grid with 800×800 grid cells.*

rotated grid method for regular grid cells and the rotated grid embedded boundary method along the boundary. For the fine discretization used here, with 800×800 grid cells on the rectangular computational domain, we have many very small cut cells, the smallest of which is about 10^{-5} times the size of a regular grid cell. However, this does not cause any stability or accuracy problem. In Table 3.1 we show results of a convergence study, comparing the solution inside the domain as well as along
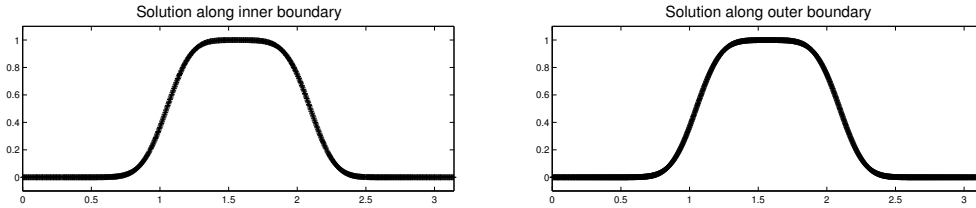
FIG. 3.3. *Solution of the annulus test problem along the inner and outer boundary after one rotation for $0 \leq \theta \leq \pi$.*

the boundaries with the exact solution. One can see that the highest accuracy was obtained along the outer boundary, while the lowest accuracy was obtained along the inner boundary. This may not be surprising, since the solution profile is resolved with more points per transition layer as the radius increases.

$mx \times my$ / EOC	domain	outer boundary	inner boundary
100×100	7.50839d-2	3.87471d-2	0.13909
200×200	2.03198d-2	1.01406d-2	4.01216d-2
EOC	**1.88**	**1.93**	**1.79**
400×400	5.14101d-3	2.56584d-3	1.02206d-2
EOC	**1.98**	**1.98**	**1.97**
800×800	1.29810d-3	6.45543d-4	2.56709d-3
EOC	**1.99**	**1.99**	**1.99**

TABLE 3.1
Convergence study for annulus test problem.

Note that advective transport inside an annulus was also studied in Calhoun and LeVeque [7], where a Cartesian grid embedded boundary method for the advection diffusion equation was developed. Their method remains stable in the case of pure advection. However, in the advection case the accuracy at the boundary was reduced, which caused an unphysical boundary layer.

Numerical convergence studies can also be found in Pember et al. [32] as well in Forrer and Jeltsch [16]. Those tests document a loss of accuracy at the boundary of those earlier Cartesian grid embedded boundary methods.

3.2. Euler equations. In order to obtain an embedded boundary method for the Euler equations we construct in addition to the h-boxes in the ξ-direction also h-boxes in the η-direction. At the boundary segment, which is a straight line for each cut cell, we construct a boundary h-box normal to the boundary. The length of this h-box is again determined by Equation (2.11), where (u, v) may now represent the normal vector at the boundary. As depicted in Figure 3.1a, we construct a boundary h-box that points into the flow domain (the *inbox*) as well as one that points into the boundary (the *outbox*). The conserved quantities assigned to the outbox are the reflected values of the conserved quantities of the inbox. For the Euler equations this means that for a vector of conserved quantities (given in Cartesian coordinates) we first determine (by rotation) the normal and tangential velocity in (ξ, η)-coordinates. We denote those velocities by $\tilde{u}$ and $\tilde{v}$. The outbox values are then obtained from the

inbox values by setting

$$\rho_{outbox} = \rho_{inbox}, \tilde{u}_{outbox} = -\tilde{u}_{inbox}, \tilde{v}_{outbox} = \tilde{v}_{inbox}, p_{outbox} = p_{inbox}$$

This is a widely used procedure to obtain boundary fluxes that simulate a reflecting boundary, see for instance [25]. It allows us to calculate the boundary flux by using the same Riemann solver routines that are used inside the computational domain. In a typical situation, where a reflecting boundary is aligned with a grid cell interface, the outbox would be called a *ghost cell*. The conserved quantities assigned to the inbox are obtained in the same way as described before for the h-boxes in the ξ-direction. For each grid cell that is overlapped by the inbox we calculate a polygon that represents the intersection of the inbox with this grid cell. We then reconstruct the conserved quantities at the center of mass of each of these polygons and calculate an area-weighted average, which is equivalent to a piecewise linear interpolation of the conserved quantities at the center of mass of the inbox.

It remains to calculate the h-box values in the η-direction at the cell interfaces near the boundary, as indicated in Figure 3.1b and c. The calculation of the conserved quantities assigned to the h-boxes that point into the flow domain follows the procedure used for the calculation of the values assigned to the inbox as well as the h-boxes in the ξ-direction. The conserved quantities assigned to the h-box that points toward the boundary is slightly more complicated. A fraction of this h-box can be inside the boundary. We first calculate the part of the h-box that intersects with the boundary and lies outside the flow domain. This polygon is then reflected at the boundary segment. For the reflected polygon we can now calculate the intersection with grid cells that are overlapped by this polygon. We then calculate a linear interpolation of the conserved quantities at the center of mass of the reflected polygon. This vector of conserved quantities is reflected and assigned to the part of the h-box that lies inside the boundary. For the fraction of the h-box that lies inside the flow domain we also calculate a linear interpolation of the conserved quantities at the center mass of this polygon. The area weighted average of conserved quantities that are assigned to those two polygons is used as the h-box value. Note that depending on the geometry of the embedded boundary a part of an h-box constructed in the ξ-direction might also intersect with the boundary, in this case we proceed as described above for h-boxes in the η-direction.

Once the h-box values are defined, we calculate fluxes at the cell interfaces of a cut cell using the same rotated grid predictor-corrector method as outlined in section 2.4. Note that this also includes the calculation of transverse flux differences. In order to calculate the transverse flux differences we define vectors Q_1, Q_2 and Q_3 of the conserved quantities, compare with section 2.4. Here Q_2 is again the h-box value. The other two points lie in the orthogonal direction a distance h away from the center of mass of the h-box. If those two points are inside the computational domain, then linear interpolation between neighboring grid cells is used to assign the values Q_1 and Q_3. If one or both of the points that are constructed in the orthogonal direction are outside the domain, then we first calculate the reflected point (which is inside the flow domain). We assign a vector of conserved quantities to the reflected point. The vector used in the calculation of the transverse flux difference can be obtained by reflection of the conserved quantities.

Below the performance of our embedded boundary method is demonstrated for shock reflection from a wedge as well as shock reflection from a cylinder.

Shock reflection from a wedge. Here we study the approximation of a Mach 10 shock wave reflected from a 30 degree wedge. The state in front of the shock is
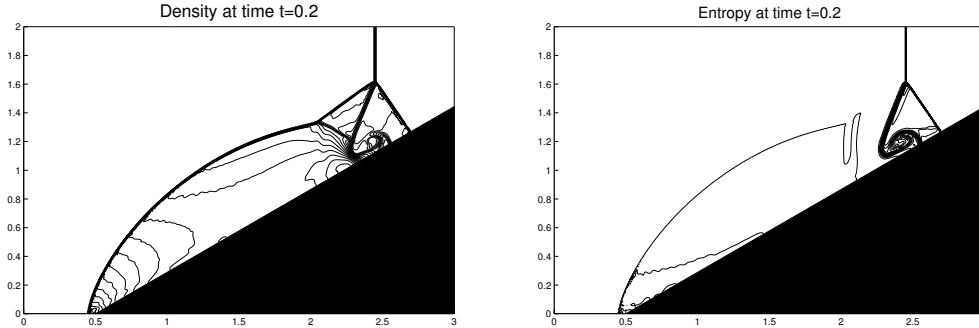

FIG. 3.4. *Shock reflection from a 30 degree wedge. Parameter values: mx= 450, my = 300, size of the smallest cut cell 4.2×10^{-6}, high-resolution rotated grid method with minmod limiter, $CFL \leq 1$. Away from the boundary the coordinate direction is aligned with the grid and no rotation is used.*

$\rho = 1.4$, $u = v = 0$, $p = 1$. At the embedded boundary we use a rotated grid which is aligned with the boundary. Inside the domain we use the grid-aligned multidimensional upwind method of Colella. For this test case the size of the smallest cut cell was 4.2×10^{-6} times the size of a regular grid cell. This did not cause any stability problem and moreover we get an accurate approximation near the boundary as well as in the whole domain. Figure 3.4 shows numerical results for density and entropy.

Shock reflection from a cylinder. Finally we consider the performance of our embedded boundary method for the Euler equations in the presence of a curved boundary. As a numerical test calculation we consider shock reflection from a circular cylinder. Initially a Mach 2 shock is located at $x = -0.3$. The state in front of the shock is again $\rho = 1.4$, $u = v = 0$, $p = 1$. Figure 3.5a, b shows contour plots for pressure and density obtained by our Cartesian grid embedded boundary method.

We determine the direction of the rotated grid at each cut cell interface such that the ξ-direction is tangential to the boundary. A smooth transition from the rotated grid to the mesh-aligned grid for grid cells near the boundary was used. In Figure 3.5c, d, we show results for the same test problem obtained by the curvilinear version of CLAWPACK [19], see LeVeque [25] for a description of the algorithm. This uses a logically rectangular grid with 90×360 grid cells, i.e. the inner boundary is resolved by 360 full cells. Although a curvilinear grid is of course a very good choice for this simple situation, we can see from this comparison that our embedded boundary method also leads to an accurate approximation of the solution structure.

In order to further study the accuracy of the embedded boundary method, we also compare the solution along the boundary, i.e. the solution in the cut cells obtained by our embedded boundary method and the solution along the first row of grid cells for the curvilinear grid cells. This comparison is shown in Figure 3.6 for a quite coarse grid, i.e. 60 cells along the boundary (cut or full respectively). Note that in order to make comparisons easier, the grids are much coarser than the ones used for the calculation shown in Figure 3.5. Again we can see that our embedded boundary method leads to an accurate approximation. It is noticeable however, that the curvilinear grid method leads to a sharper approximation of the shock wave. Such a behavior was already observed for our one-dimensional irregular grid h-box method
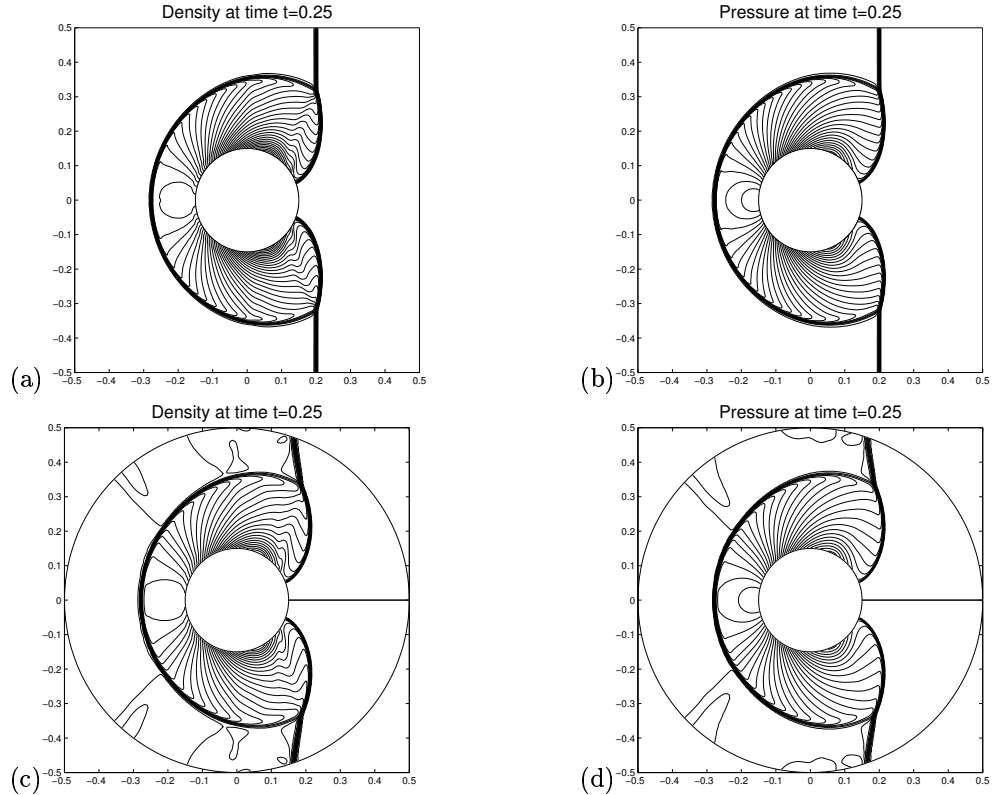
FIG. 3.5. *Reflection of a Mach 2 shock wave from a circular cylinder. (a), (b) Density and pressure obtained on Cartesian grid with* 300×300 *grid cells, 364 cut cells. (c), (d) Density and pressure for curvilinear grid method on a* 90×360 *mesh. Note that on a curvilinear grid the shock is not aligned with the mesh. Therefore, simple extrapolating boundary conditions (used here) can cause some weak waves that are moving back into the computational domain.*

presented in [2]. Since several h-boxes may overlap a single discontinuity, the method can have more smearing than usually observed on a regular Cartesian grid.
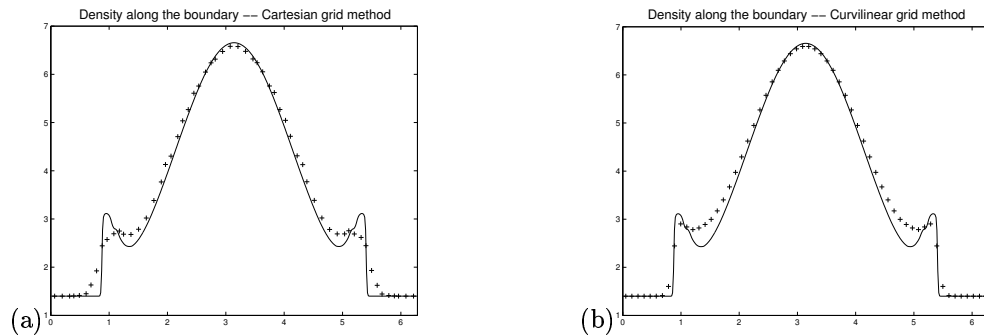

FIG. 3.6. *Density along the boundary for reflection of Mach 2 shock from a cylinder. Solution is shown for time* $t = 0.2$. *(a) Cartesian grid method on a* 50×50 *grid with* 60 *cut cells along the boundary; (b) curvilinear grid with* 60 *regular grid cells along the boundary. The solid line is a reference solution obtained by a curvilinear grid calculation on a fine mesh.*

As soon as the geometry becomes more complex, the construction of a body fitted logically rectangular mesh becomes more difficult. This is for instance the case in our last test problem, where we consider Mach reflection from two circular cylinders. The Cartesian grid embedded boundary method can of course handle such a situation. Contour plots of the pressure obtained with our Cartesian grid embedded boundary method are shown in Figure 3.7.
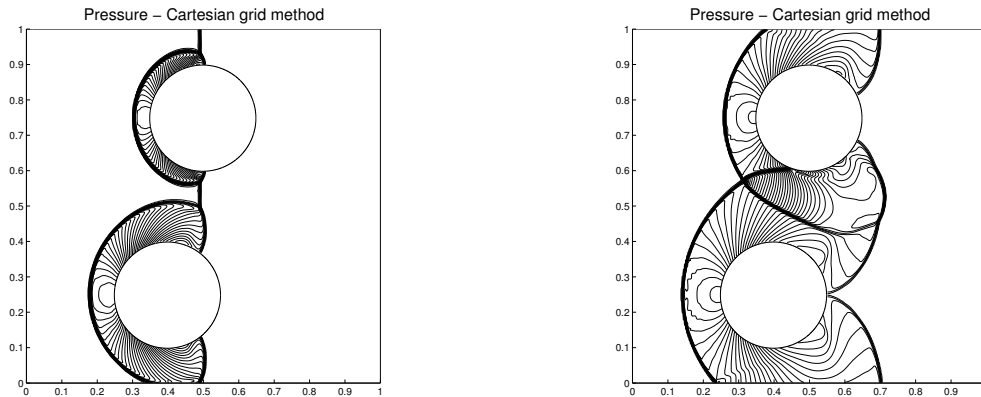

FIG. 3.7. *Reflection of a Mach 3 shock wave from two circular cylinders. Contour plots of pressure at two different time steps (t=0.096, t=0.16) calculated on an underlying Cartesian grid with* 300×300 *mesh cells. Initially a Mach 3 shock was located at* $x = 0.2$.

There has been recent work on the general problem of implementing boundary conditions at curved boundaries, for example see Dadone and Grossman [11], [12] for modifications of the usual technique for using ghost cells for reflecting boundaries cells for steady state problems. We expect that similar improvements for boundary conditions at curved reflecting boundaries could be incorporated into our h-box implementation at curved boundaries as well. We plan to investigate this further for both curvilinear grids as well as for our Cartesian grid embedded boundary method. A higher order representation of the geometry may also be necessary in order to further increase the accuracy, see also [1].

4. Conclusions. We developed a high-resolution rotated grid h-box method, which is second order accurate for smooth solutions of conservation laws and prevents unphysical oscillations near discontinuities. This method was incorporated in a Cartesian grid embedded boundary method. The resulting method leads to a stable, accurate and conservative approximation of conservation laws in the presence of irregular embedded boundaries. Our new rotated grid h-box method is more accurate than other existing Cartesian grid embedded boundary methods for conservation laws. In order to further increase the accuracy at the boundary, it would be interesting to study boundary treatments that use a higher-order representation of the boundary. In our current approach the boundary segment is approximated piecewise linearly in each cut cell. Higher accuracy with the current approach can also be obtained by adaptive mesh refinement. By using different patches of Cartesian grids (as for instance described in [3]), we can apply our embedded boundary treatment on every level of refinement in exactly the same form as described in this paper for a single grid.

REFERENCES

[1] F. Bassi and S. Rebay. High-order accurate discontinous finite element solution of the 2D Euler equations. *J. Comput. Phys.*, 138:251–285, 1997.

[2] M.J. Berger, C. Helzel, and R.J. LeVeque. *h*-box methods for the approximation of hyperbolic conservation laws on irregular grids. *SIAM J. Numer. Anal.*, 41:893–918, 2003.

[3] M.J. Berger and R.J. LeVeque. An adaptive Cartesian mesh algorithm for the Euler equations in arbitrary geometries. *AIAA paper AIAA-89-1930*, pages 305–311, 1989.

[4] M.J. Berger and R.J. LeVeque. Stable boundary conditions for Cartesian grid calculations. *Computing Systems in Engineering*, 1:305–311, 1990.

[5] M.J. Berger and R.J. LeVeque. A rotated difference scheme for Cartesian grids in complex geometries. *AIAA Paper CP-91-1602*, 1991.

[6] M.J. Berger, R.J. LeVeque, and L.G. Stern. Finite volume methods for irregular one-dimensional grids. In *Mathematics of Computation 1943-1993: a half century of computational mathematics, Proc. of Symposia in Applied Mathematics*, volume 48, pages 255–259, 1994.

[7] D. Calhoun and R.J. LeVeque. A Cartesian grid finite-volume method for the advection diffusion equation in irregular geometries. *J. Comput. Phys.*, 157:143–180, 2000.

[8] I.-L. Chern and P. Colella. A conservative front tracking method for hyperbolic conservation laws. Preprint Lawrence Livermore National Lab, UCRL-97200, 1987.

[9] W.J. Coirier and K.G. Powell. An accuracy assessment of Cartesian-mesh approaches for the Euler equations. *J. Comput. Phys.*, 117:121–131, 1995.

[10] P. Colella. Multidimensional upwind methods for hyperbolic conservation laws. *J. Comput. Phys.*, 87:171–200, 1990.

[11] A. Dadone. Symmetry techniques for the numerical solution of the 2d Euler equations at impermeable boundaries. *Int. J. Numer. Meth. Fluids*, 28:1093–1108, 1998.

[12] A. Dadone and B. Grossman. Surface boundary conditions for the numerical solution of the Euler equations. *AIAA Journal*, 32:285–293, 1994.

[13] S.F. Davis. A rotationally biased upwind difference scheme for the Euler equations. *J. Comput. Phys.*, 56:65–92, 1984.

[14] J. Falcovitz, G. Alfandary, and G. Hanoch. A two-dimensional conservation laws scheme for compressible flows with moving boundaries. *J. Comput. Phys.*, 138:83–102, 1997.

[15] H. Forrer and M.J. Berger. Flow simulations on Cartesian grids involving complex moving geometries. In M. Fey and R. Jeltsch, editors, *Proc. Int. Conf. Hyperbolic Problems*, 1998.

[16] H. Forrer and R. Jeltsch. A high-order boundary treatment for Cartesian-grid methods. *J. Comput. Phys.*, 140:259–277, 1998.

[17] B. Gustafsson. The convergence rate for difference approximations to mixed initial boundary value problems. *Math. Comp.*, 29:396–406, 1975.

[18] A. Jameson. Iterative solution of transonic flow over airfoils and wings, including flows at Mach 1. *Comm. Pure. Appl. Math*, 27(3):283–309, 1974.

[19] R.J. LeVeque. CLAWPACK software. available from http://www.amath.washington.edu/~rjl/clawpack.html.

[20] R.J. LeVeque. Large time step shock-capturing techniques for scalar conservation laws. *SIAM J. Numer. Anal.*, 19:1091–1109, 1982.

[21] R.J. LeVeque. Convergence of a large time step generalization of godunov's method for conservation laws. *Comm. Pure Appl. Math.*, 37:463–477, 1984.

[22] R.J. LeVeque. A large time step generalization of Godunov's method for systems of conservation laws. *SIAM J. Num. Anal.*, 22:1051–1073, 1985.

[23] R.J. LeVeque. High-resolution conservative algorithms for advection in incompressible flow. *SIAM J. Numer. Anal.*, 33:627–665, 1996.

[24] R.J. LeVeque. Wave propagation algorithms for multidimensional hyperbolic systems. *J. Comput. Phys.*, 131:327–353, 1997.

[25] R.J. LeVeque. *Finite Volume Methods for Hyperbolic Problems*. Cambridge University Press, 2002.

[26] R.J. LeVeque and R. Walder. Grid alignment effects and rotated methods for computing complex flows in astrophysics. In *Proc. GAMM Conf. on Comput. Fluid Dyn., Lausanne*, 1991.

[27] D.W. Levy, K.G. Powell, and B. van Leer. Use of a rotated Riemann solver for the two-dimensional Euler equations. *J. Comput. Phys.*, 106:201–214, 1993.

[28] R. Liska and B. Wendroff. Comparison of several difference schemes on 1d and 2d test problems for the Euler equations. *SIAM J. Sci. Comput.*, 25:995–1017, 2003.

[29] D. Modiano and P. Colella. A higher-order embedded boundary method for time dependent

simulation of hyperbolic conservation laws. In *Proceedings of the FEDSM 00 - ASME Fluids Engineering Simulation Meeting*, 2000.

[30] K.W. Morton. On the analysis of finite volume methods for evolutionary problems. *SIAM J. Numer. Anal.*, 35:2195–2222, 1998.

[31] S.M. Murman, M.J. Aftosmis, and M.J. Berger. Impicit approaches for moving boundaries in a 3-d cartesian method, 2003. AIAA 2003-1119, 41st AIAA Meeting.

[32] R.B. Pember, J.B. Bell, P. Colella, and W.Y. Crutchfield amd M.L.Welcome. An adaptive Cartesian grid method for unsteady compressible flow in irregular regions. *J. Comput. Phys.*, 120:278–304, 1995.

[33] J.J. Quirk. An alternative to unstructured grids for computing gas dynamic flows around arbitrarily complex two-dimensional bodies. *Computers Fluids*, 23:125–142, 1994.

[34] P.L. Roe and D. Sidilkover. Optimum positive linear schemes for advection in two and three dimensions. *SIAM J. Numer. Anal.*, 29:1542–1568, 1992.

[35] C.W. Schultz-Rinne, J.P. Collins, and H.M. Glaz. Numerical solution of the Riemann-problem for two-dimensional gas dynamics. *SIAM J. Sci. Comput.*, 14:1394–1414, 1993.

[36] D. Sidilkover and A. Brandt. Multigrid solution to steady-state two-dimensional conservation laws. *SIAM J. Numer. Anal.*, 30:249–274, 1993.

[37] D. Sidilkover and P.L. Roe. Unification of some advection schemes in two dimensions, 1995. ICASE Technical Report 95-10.

[38] S. Xu, T. Aslam, and D.S. Stewart. High resolution numerical simulation of ideal and non-ideal compressible reacting flows with embedded internal boundaries. *Combust. Theory Modelling*, 1:113–142, 1997.